

Lithographically patterned wires of the charge-density-wave conductor $\text{Rb}_{0.30}\text{MoO}_3$

O. C. Mantel, C. A. W. Bal, C. Langezaal, C. Dekker,
and H. S. J. van der Zant^{a)}

Department of Applied Physics and DIHES, Delft University of Technology, Lorentzweg 1, 2628 CJ Delft, The Netherlands

(Received 29 March 1999; accepted for publication 8 July 1999)

We have developed a technology for the patterning of thin films of the charge-density-wave (CDW) conductor $\text{Rb}_{0.30}\text{MoO}_3$. By means of photolithography and Ar-ion milling, wire structures are defined in the films. The $\text{Rb}_{0.30}\text{MoO}_3$ wires are contacted by (sub)micron Au contacts, which are fabricated by optical and electron-beam lithographic techniques. Electrical transport measurements clearly demonstrate the CDW state in our patterned structures, including CDW sliding. Patterned wires enable the study of CDWs on mesoscopic length scales. © 1999 American Institute of Physics. [S0021-8979(99)00520-4]

I. INTRODUCTION

The charge-density-wave (CDW) state occurs in conductors with a strongly anisotropic crystal structure.¹ In such conductors, electron-phonon interactions induce a transition to a new collective ground state, in which the electron density is periodically modulated. Above a certain applied electric field, CDWs can be depinned from impurities and move through the lattice. This “sliding” of CDWs causes several unusual electrical transport effects, such as strongly nonlinear $I(V)$ characteristics, an ac voltage response to an applied dc current, and memory effects at low temperatures.

The CDW state shows strong analogies to the superconducting state. The CDW transition can be viewed as a Bose condensation of electron-hole pairs, similar to Cooper-pair formation in superconductors. Several CDW properties can be described with equations for superconductors, with the role of current and voltage reversed. A linear current-frequency relation exists, for instance, which is the equivalent of the well-known ac Josephson relation. Thin-film devices with Josephson junctions are used for both fundamental studies and commercial applications. Even for the more complex high- T_C superconductors, a thin-film technology has been developed and micron-size heterostructures have been fabricated. For CDW conductors, this type of technology has not yet been reported.

New effects are expected in CDW systems of (sub)micron dimensions. X-ray experiments have shown^{2,3} that the phase of a CDW can be coherent over a distance of several micrometers. The theoretical study of phase-coherent CDW systems has resulted in several remarkable predictions.⁴⁻⁶ For instance, dissipationless currents can flow through the normal region N in a CDW-N-CDW junction. Gate-modulated transport in a CDW electron pump has also been reported.⁶ Such a pump consists of a CDW dot between two normal regions and a third electrode which is capacitively coupled to the dot. A controlled study of these effects be-

comes feasible with thin films. These films can be patterned by lithographic techniques, thus allowing definition of structures of arbitrary shapes.

In an earlier paper, we reported the growth of thin films of a CDW conductor.⁷ By use of a pulsed-laser deposition technique, thin films of the blue bronze $\text{Rb}_{0.30}\text{MoO}_3$ were synthesized. The blue bronzes $\text{A}_{0.30}\text{MoO}_3$ ($\text{A}=\text{K}, \text{Rb}, \text{Tl}$) are among the most extensively studied CDW conductors. Their strongly anisotropic crystal structure consists of slabs of weakly linked chains of MoO_6 octahedra that are separated by alkali ions. The Peierls transition to the CDW state occurs near 180 K. Sliding-CDW transport can then occur along the chains of MoO_6 octahedra, parallel to the crystallographic b axis.

In this article we describe the next step in the development of a thin-film technology for a CDW conductor: the patterning of $\text{Rb}_{0.30}\text{MoO}_3$ films. To our knowledge, this is the first demonstration of patterned structures in thin CDW films. We will first give a brief description of the $\text{Rb}_{0.30}\text{MoO}_3$ films in Sec. II. The fabrication of narrow $\text{Rb}_{0.30}\text{MoO}_3$ wires with dimensions down to 1 μm is described in Sec. III. In Sec. IV we deal with the fabrication of CDW devices that consist of wire structures with metal contacts on top. Au contact spacings down to 100 nm have been realized. The CDW properties of the fabricated structures are discussed in Sec. V.

II. THIN FILMS OF $\text{Rb}_{0.30}\text{MoO}_3$

Thin $\text{Rb}_{0.30}\text{MoO}_3$ films are grown by pulsed-laser deposition on $\text{Al}_2\text{O}_3(012)$ (sapphire) or $\text{SrTiO}_3(100)$ substrates. The substrates are mounted on a heater block in a vacuum chamber, opposite a polycrystalline $\text{Rb}_{0.30}\text{MoO}_3$ target. A plasma is formed by shooting the target with high-energy laser pulses. Important process parameters are the substrate temperature during growth, the oxygen pressure in the chamber, the beam profile of the laser, and the pulse energy and repetition rate. A typical $\text{Rb}_{0.30}\text{MoO}_3$ film is grown at 440 °C

^{a)}Electronic mail: herre@gt.tn.tudelft.nl

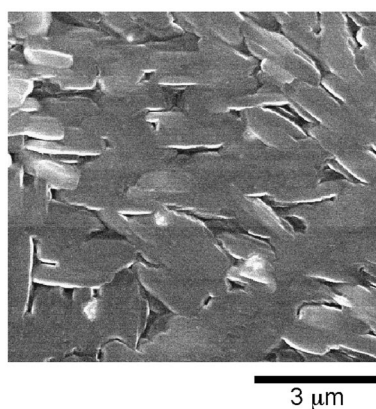


FIG. 1. SEM image of a $0.3 \mu\text{m}$ thick $\text{Rb}_{0.30}\text{MoO}_3$ film grown at 440°C on an $\text{Al}_2\text{O}_3(012)$ substrate. The film consists of grains with typical sizes of $1\text{--}3 \mu\text{m}$. X-ray analysis (not shown) confirms that the grains have a CDW sliding direction parallel to the plane of the substrate.

at 120 mTorr oxygen pressure with a pulse energy of $1 \text{ J}/\text{cm}^2$. The deposition rate is typically 0.2 nm/s .

Figure 1 shows a scanning electron microscopy (SEM) image of a $\text{Rb}_{0.30}\text{MoO}_3$ film grown on an $\text{Al}_2\text{O}_3(012)$ substrate. The film consists of grains with typical sizes of $1 \mu\text{m}$. The size of the grains is dependent on the growth temperature and the laser-pulse energy. Due to the formation of other Rb_xMoO_y phases at temperatures too high or pulse energies too low, however, the maximum grain size is limited to about a few micrometers. The surface corrugation of the films is substantial, and can be of the order of the film thickness for films grown at high temperatures ($440\text{--}460^\circ\text{C}$). $\theta\text{-}2\theta$ x-ray analysis shows that the films are $(\bar{2}01)$ oriented,⁷ i.e., the CDW conducting direction in each grain is parallel to the plane of the substrate. The orientation *within* this plane is random for films on Al_2O_3 substrates, although the grains usually group together into clusters with parallel orientation.

In-plane alignment can be obtained on $\text{SrTiO}_3(100)$ substrates. For this substrate type, the grains align with their CDW axis parallel to the axes of the $\text{SrTiO}_3(100)$ substrate surface lattice, resulting in two perpendicular orientations.⁸ This in-plane alignment would suggest that such films are more suitable for the fabrication of thin-film devices. However, we find that due to a weaker adhesion between the film and substrate, patterning of films is more difficult on SrTiO_3 substrates than on Al_2O_3 ones. Most structures have therefore been patterned in films on Al_2O_3 .

III. FABRICATION OF $\text{Rb}_{0.30}\text{MoO}_3$ WIRES

Patterning of $\text{Rb}_{0.30}\text{MoO}_3$ thin films is performed by the use of near-ultraviolet (near-UV) photolithography. A schematic representation of the process is shown in Fig. 2. In the first step, a Cu/Au sandwich is evaporated on top of the film. This sandwich serves as a coating to prevent direct contact between the film and water-based solutions during the process (in water-based solutions, films tend to peel off easily). The thickness of the Cu/Au coating is chosen to be comparable to the corrugation of the film surface to achieve full coverage of the film. Good results are obtained with a sand-

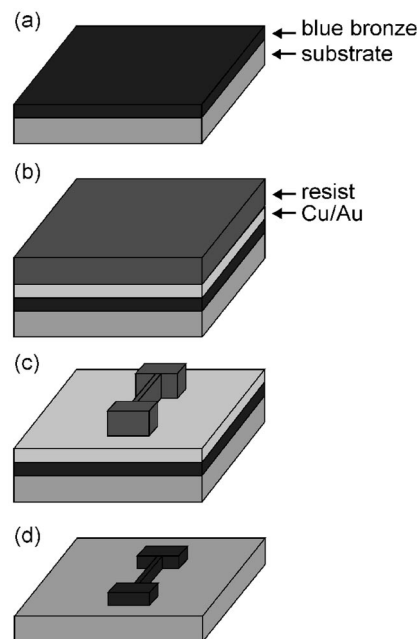


FIG. 2. Schematic representation of the process for patterning blue bronze films. (a) $\text{Rb}_{0.30}\text{MoO}_3$ film on a substrate. (b) A Cu/Au layer is evaporated to protect the film against water-based solutions. Subsequently a $1.1 \mu\text{m}$ thick layer of photoresist is applied. (c) The resist layer is exposed to near-UV light and developed. (d) The pattern is transferred to the film by Ar-ion milling through the Cu/Au layer and the film.

wich of 10 nm Cu and 150–300 nm Au. The thin Cu layer improves the adhesion between $\text{Rb}_{0.30}\text{MoO}_3$ and Au.⁹

Lithography is performed with SR1813, a positive resist sensitive to near-UV light. A thick resist layer is chosen, because the resist serves as an etch mask during Ar-ion milling. The etch rate of SR1813 resist is about $1 \mu\text{m/h}$, i.e., more than twice as high as the etch rate of $0.3\text{--}0.4 \mu\text{m/h}$ for $\text{Rb}_{0.30}\text{MoO}_3$ films. For processing a $0.3 \mu\text{m}$ thick film, a thick resist layer of at least $0.8 \mu\text{m}$ is thus required. We use a layer of $1.1 \mu\text{m}$, applied by spin coating.¹⁰ After baking at 90°C , the resist is exposed through a glass mask with a metallic pattern by means of a Karl Suzu aligner. The exposure time is 9–11 s. The exposed resist is dissolved in water-diluted Microposit developer.

Etching of the film and the Cu/Au coating is done by Ar-ion milling in a homemade Kaufmann source. Typical etch parameters are an acceleration voltage of 300 V and a beam current of $400 \mu\text{A}$, yielding an etch rate for $\text{Rb}_{0.30}\text{MoO}_3$ of $0.4 \mu\text{m/h}$. Etching of the films is a very critical process, since grains can be removed from the wires for etching times that are too long. Optimal etching results are obtained as follows. In the first step, the Cu/Au coating and the $\text{Rb}_{0.30}\text{MoO}_3$ films are etched until the bare sapphire substrate is visible. After this etching, some remnants of resist are still present on top of the defined structures. These are first removed in warm acetone. Then, in the second etching step, the Cu/Au layer on top of the structures is etched at a rate of $2 \mu\text{m/h}$. It is generally not possible to remove all of the Cu/Au by Ar-ion milling due to some redeposition, which occurs particularly at the edges of the patterned structures. Redepleted Au, which may otherwise shortcircuit the

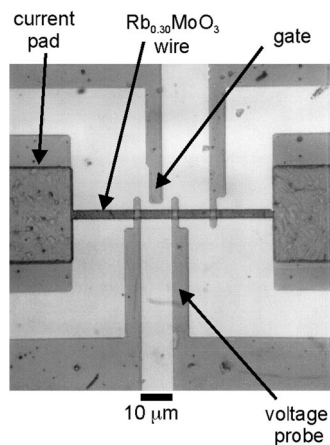


FIG. 3. Optical microscope image of a $2.5 \mu\text{m}$ wide blue bronze wire with Au contacts. Current is injected at the large pads at the ends of the wire. In the middle, three voltage probes are connected to the wire. A fourth, wider probe can be used as a gate electrode.

wire, is removed by dipping the sample in a water-based solution of KI/I_2 for a few seconds. Although wires may come loose during dipping, we find that this wet etching is the best method for removing redeposited Au.

By using the above process, wires with widths down to $1 \mu\text{m}$ can be fabricated in a controlled way.

IV. FABRICATION OF $\text{Rb}_{0.30}\text{MoO}_3$ DEVICES

To fabricate CDW devices, metal contacts have to be connected to the $\text{Rb}_{0.30}\text{MoO}_3$ wire structures. For the definition of Au contacts, both optical and electron-beam lithography have been employed. In Sec. IV A we describe micron-size devices for which the contacts are defined by near-UV optical lithography. The fabrication of submicron Au contacts by electron-beam lithography is discussed in Sec. IV B.

A. Optical lithography

For the definition of micron-size Au contact wires, we use a process analogous to the process for fabricating the blue bronze structures, i.e., first a Cu/Au sandwich is evaporated, then a resist pattern is defined on top, and subsequently a pattern is etched into the Cu/Au layer by Ar-ion milling. Step coverage of the metal across the blue bronze wire edge is achieved when a Cu/Au layer thickness of 150–200 nm is used.

A typical example of a wire structure fabricated by near-UV lithography is shown in Fig. 3. It consists of a $0.3 \mu\text{m}$ thick $\text{Rb}_{0.30}\text{MoO}_3$ wire with a width of about $2.5 \mu\text{m}$. At the ends of the wire, $30 \times 30 \mu\text{m}^2$ squares are defined to ensure low contact resistance for current injection. Note that the granular structure of the $\text{Rb}_{0.30}\text{MoO}_3$ film is visible within these areas. The Au contacts overlap the square current pads at the ends of the wire. Near the middle, three voltage probes are connected. At the places where they contact the wire, their width is only $2 \mu\text{m}$. A fourth, wider Au structure does not connect to the wire, because it is intended for use as a gate electrode.¹¹

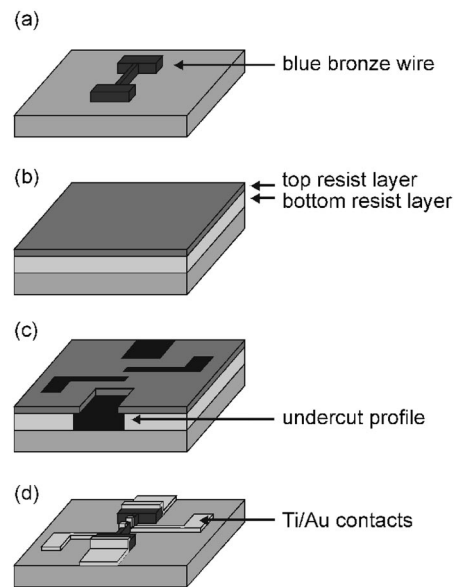


FIG. 4. Schematic representation of a lift-off process for defining submicron metal contacts on top of $\text{Rb}_{0.30}\text{MoO}_3$ wires. (a) Blue bronze wire structure. (b) A double layer of electron-beam resist is spin coated on top of the wire. (c) The resist is exposed and developed, resulting in an undercut profile. (d) A Ti/Au layer is evaporated, which after liftoff only remains at the places where the resist had been developed.

By using near-UV optical lithography, we have made $\text{Rb}_{0.30}\text{MoO}_3$ wire structures with varying dimensions. The minimum voltage-probe spacing that can be achieved with this technique is about $1 \mu\text{m}$.

B. Electron-beam lithography

By using electron-beam lithography, we have realized submicron voltage contacts with spacings down to 100 nm on top of $\text{Rb}_{0.30}\text{MoO}_3$ wires. The use of PMMA/MMA electron-beam resist that is not water based makes it possible to perform a “lift-off” process. In this method, one first applies resist, then evaporates metal at the places where the resist has been developed, and finally removes the resist (lift-off). Such a process is difficult to use for the definition of contacts on $\text{Rb}_{0.30}\text{MoO}_3$ wires by near-UV lithography when direct contact between the wires and water-based photoresist developer should be avoided. PMMA/MMA resist, on the other hand, is developed in methylisobutyl ketone (MIBK) and propanol, which do not significantly affect the adhesion of the $\text{Rb}_{0.30}\text{MoO}_3$ wires.

A schematic representation of the electron-beam patterning process is depicted in Fig. 4. First, a double layer of 300 nm PMMA/MMA and 50 nm PMMA electron-beam resist is spin coated onto the sample and baked at 180°C . Subsequently, a 20 nm Au coating (not shown in Fig. 4) is sputtered on top to prevent charging of the insulating Al_2O_3 substrate during exposure. We find that this sputtered coating does not affect the development process of the electron-beam resist after exposure. The exposed resist can still dissolve, and probably vanishes through small cracks in the Au coating. The coating is later removed by 30 s Ar-ion milling prior to evaporation of the Ti/Au metal contact layer.

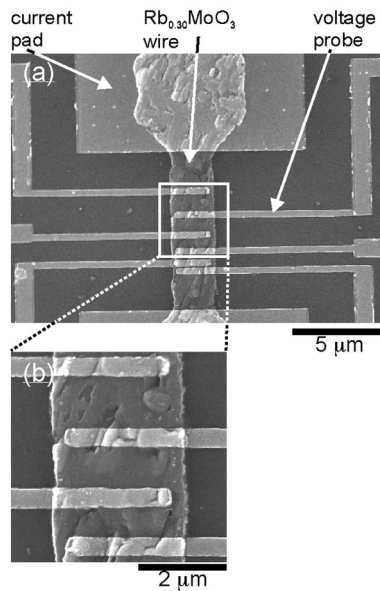


FIG. 5. (a) SEM image of a blue bronze wire structure with electron-beam-patterned gold contacts. The voltage probes are 400 nm wide. The spacings between adjacent voltage probes are, from top to bottom, 1.1, 0.85, 0.6, 0.35, and 0.1 μm . (b) Blowup of the middle part of the structure.

Exposure of the resist is done with a Leica HR5 electron-beam pattern generator (100 kV). The contact pattern can be aligned to the wire to within 100 nm by use of markers patterned into the $\text{Rb}_{0.30}\text{MoO}_3$ film. After exposure, the resist is developed for 1 min in a 1:3 mixture of MIBK and 2-propanol. The polymers in the thicker bottom layer have a smaller molecular weight, and are better dissolved after electron-beam exposure. In this way, an undercut profile is created in the double-layer resist [Fig. 4(c)].

The thickness of the evaporated Ti/Au metal layer should be chosen carefully, because the metal contacts must be continuous across the edge of the $\text{Rb}_{0.30}\text{MoO}_3$ wire structure. This step coverage is most easily obtained if a contact layer as thick as possible is chosen. On the other hand, for successful liftoff of the metal, a thin layer is required. We obtain the best results with a layer of 60 nm Au, which is partly evaporated under an angle of 20° with respect to the surface normal. A 10 nm thick layer of Ti is evaporated as an adhesive layer between $\text{Rb}_{0.30}\text{MoO}_3$ and Au. Liftoff is performed in boiling acetone.

Figure 5 shows a SEM image of a wire structure in which the Au contacts have been defined by electron-beam lithography. The width of the $\text{Rb}_{0.30}\text{MoO}_3$ wire is $2.8 \mu\text{m}$. The wire is connected by six voltage probes at different spacings. Note that a mutual distance between probes of as small as only 100 nm can be realized. For most devices, good step coverage is obtained. An example is shown in Fig. 6, which shows a high-magnification SEM image of a voltage probe at a wire edge. The edge of the blue-bronze wire is very steep. Nonetheless, the Au angle-evaporation technique has been successful in realizing step coverage.

V. CDW CHARACTERISTICS OF PATTERNED WIRES

The CDW characteristics of patterned $\text{Rb}_{0.30}\text{MoO}_3$ wires have been studied by use of electrical transport measure-

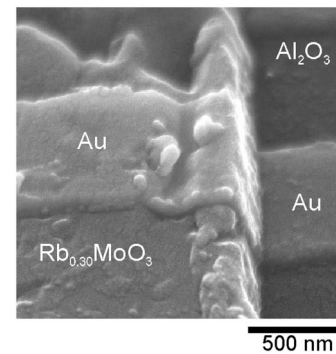


FIG. 6. Tilted SEM image of a $\text{Rb}_{0.30}\text{MoO}_3$ wire edge. Adequate step coverage of the Au probe is obtained. Along the wire edge some redeposited $\text{Rb}_{0.30}\text{MoO}_3$ is visible.

ments. Those wires that have room-temperature resistivity comparable to the value along b for bulk crystals are selected. Such wires show deviations from bulk behavior. The mechanism for CDW pinning is different, resulting in higher depinning fields. Below about 50 K, the electrical properties change, which is consistent with a transition to motion of CDW deformations as the mainly responsible transport mechanism. A detailed comparison between the electrical transport properties of the wire structures and data for bulk crystals will be reported in a separate paper.¹² Here, we discuss some basic electrical properties of the wires that demonstrate the existence of a CDW state.

The wires are measured in a four-terminal configuration, i.e., current is injected at the current pads at the ends of the wire and voltage is measured with the small voltage probes near the middle. Contact resistances of the small voltage probes are determined by use of three-terminal measurements. In such measurements, the contact resistance of contact B of three adjacent contacts A , B , and C is determined by applying current between A and B and measuring the resulting voltage between B and C .

The low-bias contact resistance of the small voltage probes ranges from 0.1 to 10 k Ω at room temperature, and from 0.01 to 1 M Ω at 70 K. The contact resistance of the small probes strongly decreases with increasing bias current. This nonlinearity is particularly important at low temperatures, and occurs most strongly for the smallest contacts defined by electron-beam lithography. At 70 K, we observe a decrease by typically a factor of 5 for the differential resistance of a small contact if 100 mV is applied over this contact. The nonohmic behavior of the small contacts makes them less suitable for current injection.

The room-temperature resistivity of measured $\text{Rb}_{0.30}\text{MoO}_3$ wires varies between 1 and 500 m Ω cm. This wide range of values is explained by the random in-plane orientation of the CDW chains on Al_2O_3 substrates and the presence of grain boundaries in the wires. The lowest measured resistivities of 1 m Ω cm are in good agreement with the resistivity of bulk $\text{Rb}_{0.30}\text{MoO}_3$ crystals along the CDW conducting direction.^{13,14} For the perpendicular direction (but still with the CDW chains within the substrate plane) the $\text{Rb}_{0.30}\text{MoO}_3$ resistivity is 20–80 m Ω cm. For the study of sliding-CDW transport, we select only those wires with

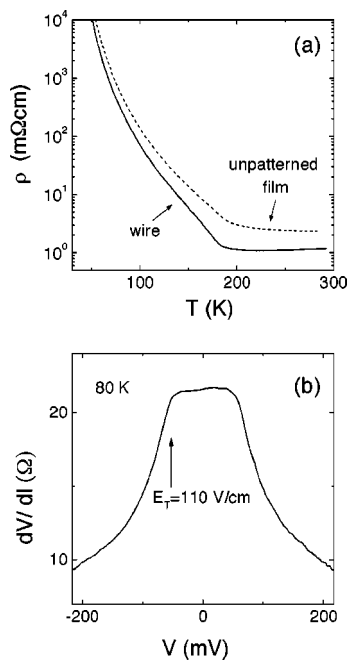


FIG. 7. (a) Resistivity vs temperature for a 5 μm long blue bronze wire segment and for an unpatterned film with 500 μm spaced contacts. A transition to the CDW state is observed near 180 K. (b) Differential resistance vs voltage for the wire segment. A sharp decrease of dV/dI near $V=50$ mV marks the onset of CDW sliding.

room-temperature resistivity smaller than 5 m Ω cm.

The patterned $\text{Rb}_{0.30}\text{MoO}_3$ wires show a clear transition to the CDW state, with a Peierls gap comparable to the gap for bulk crystals. Figure 7(a) shows the resistivity versus temperature $\rho(T)$ for a 2 μm wide patterned wire. For comparison, we have also plotted $\rho(T)$ for an unpatterned film with 500 μm spaced contacts, applied by Au evaporation through a mechanical mask. The room-temperature resistivity of the wire is 1.2 m Ω cm. Upon cooling, the resistivity first slightly decreases, which is the expected metal-like behavior for conduction along the b axis. Near 180 K, a sharp increase in resistivity is observed, consistent with the opening of a gap at the Fermi level. The data below 180 K can be fitted with a function describing the thermally activated excitation of quasiparticles across the Peierls gap $\Delta(T)$. We find $\Delta(0)=44$ meV for the wire, in good agreement with reported values on bulk crystals.^{14,15} For the unpatterned film, a similar Peierls transition to a state with a comparable energy gap [$\Delta(0)=41$ meV] is observed. Note, however, that the room-temperature resistivity for the unpatterned film is higher, and that no metal-like behavior is found above 180 K. These features are attributed to the granular nature of the film. For an unpatterned film with 500 μm spaced contacts, current flows through many grains with different in-plane orientations. The $\rho(T)$ curve for the film therefore reflects the properties of many differently oriented grains, as well as the effect of grain boundaries. Better CDW characteristics are obtained in patterned wires.

Sliding-CDW transport in the wires is demonstrated by recording the differential resistance dV/dI versus voltage. Figure 7(b) shows dV/dI at 80 K. At low fields, the differential resistance has a constant value of 22 k Ω , consistent

with a situation in which the CDW is pinned and the resistance is due to thermally excited quasiparticles. At a threshold voltage $V_T=53$ mV, a sharp decrease of dV/dI marks the onset of CDW sliding. The corresponding threshold field $E_T=110$ V/cm is one to two orders of magnitude larger than that for single crystals of comparable thickness.¹⁶ Such high E_T values indicate that the CDW is strongly pinned.

The high threshold fields for sliding imply that considerable current densities are required to measure sliding-CDW behavior. At 70 K, the typical bias current is 10 μA , corresponding to a current density of about 10 A/mm². We find that these high current densities do not destroy our wires and that they cause no significant heating in the normal four-terminal geometry. Heating effects can, on the other hand, be present when current is injected through the small contacts. At 70 K, such heating occurs if the power dissipated at the contacts exceeds typically 10 μW .

VI. CONCLUSION

We have developed a thin-film patterning technology for a CDW conductor. By using lithographic techniques, wire structures are patterned in laser-deposited thin films of $\text{Rb}_{0.30}\text{MoO}_3$. The thin-film CDW devices have been realized by contacting the wires with submicron Au contacts with spacings down to 100 nm. The wires show the Peierls transition near 180 K to a CDW state with a bulk-like energy gap. CDW sliding is observed below 180 K. The good CDW characteristics indicate that the patterning process has not significantly affected the $\text{Rb}_{0.30}\text{MoO}_3$ material.

ACKNOWLEDGMENTS

The authors wish to acknowledge Anja van Langen-Suurling for help with electron-beam patterning. This work was supported by the Netherlands Foundation for Fundamental Research on Matter (FOM). One of the authors (H.S.J.vdZ.) was supported by the Dutch Royal Academy of Arts and Sciences (KNAW).

¹For a review on CDWs, see, for example, G. Grüner, *Density Waves in Solids* (Addison-Wesley, Reading, MA, 1994).

²E. Sweetland, C.-Y. Tsai, B. A. Wintner, J. D. Brock, and R. E. Thorne, *Phys. Rev. Lett.* **65**, 3165 (1990).

³S. M. DeLand, G. Mozurkewich, and L. D. Chapman, *Phys. Rev. Lett.* **66**, 2026 (1991).

⁴M. I. Visscher and G. E. W. Bauer, *Phys. Rev. B* **54**, 2798 (1996).

⁵M. I. Visscher and B. Rejaei, *Phys. Rev. Lett.* **79**, 4461 (1997).

⁶M. I. Visscher, Ph.D. thesis, Delft University of Technology, 1998.

⁷H. S. J. van der Zant, O. C. Mantel, C. Dekker, J. E. Mooij, and C. Træholt, *Appl. Phys. Lett.* **68**, 3823 (1996); O. C. Mantel, H. S. J. van der Zant, A. J. Steinfort, C. Dekker, C. Træholt, and H. W. Zandbergen, *Phys. Rev. B* **55**, 4817 (1997).

⁸O. C. Mantel, H. S. J. van der Zant, A. J. Steinfort, C. Træholt, and C. Dekker, *Synth. Met.* **86**, 2193 (1997).

⁹For such adhesive layers, Ti is often used. We found, however, that Ti is not suitable in our dry-etching process. Structures that are fabricated with Ti as the interface layer remain metallic down to low temperatures, even after prolonged Ar-ion milling.

¹⁰Although the spinning procedure yields a resist layer with a homogeneous thickness over more than 80% of the sample area, a strong increase of the resist thickness is observed at the edges of the 5 \times 5 mm² substrate. These resist "walls" at the sample edges would prevent the necessary close contact between the middle of the sample and the glass mask during

near-UV exposure. Therefore, the thick resist edges are removed, prior to pattern definition, by near-UV exposure for 2 min and development.

- ¹¹The threshold field for CDW sliding can be modulated by sweeping the voltage on a nearby gate electrode, see, for example, T. L. Adelman, S. V. Zaitsev-Zotov, and R. E. Thorne, *Phys. Rev. Lett.* **74**, 5264 (1995).
- ¹²O. C. Mantel, C. A. W. Bal, C. Langezaal, C. Dekker, and H. S. J. van der Zant, *Phys. Rev. B* (to be published).
- ¹³E. Bervas, Thèse d'Ingénieur Docteur, Université Scientifique, Tech-

nologique et Médicale de Grenoble, 1984.

- ¹⁴W. Brütting, P. H. Nguyen, W. Riess, and G. Paasch, *Phys. Rev. B* **51**, 9533 (1995).
- ¹⁵C. Schlenker, J. Dumas, C. Escribe-Filippini, and H. Guyot, in *Low-Dimensional Electronic Properties of Molybdenum Bronzes and Oxides*, edited by C. Schlenker (Kluwer Academic, Dordrecht, 1989), pp. 159–257.
- ¹⁶X. M. Wang, D.-I. Zhang, and Y. Zhang, *Phys. Rev. B* **45**, 13250 (1992).